AIAA JOURNAL
Vol. 49, No. 6, June 2011

Aerodynamics of a Heaving Airfoil in Ground Effect

Juan Molina* and Xin Zhang†
University of Southampton, Southampton, England SO17 1BJ, United Kingdom

DOI: 10.2514/1.J050369

The aerodynamic behavior of an inverted airfoil in ground effect under heaving motion was investigated numerically. A sinusoidal vertical movement perpendicular to a uniform freestream was imposed on the airfoil. The response showed a periodic pattern that repeated with the same frequency as the heaving motion. The effect of reduced frequency at several mean distances from the ground was examined. By analyzing the lag of the aerodynamic coefficients with respect to the vertical motion, the flow can be classified into different regimes. Three fundamental features that define these regimes have been identified: 1) ground effect, 2) incidence effect, and 3) added mass effect. At low frequencies, the airfoil can be assumed to be in a quasi-stationary motion and the ground effect governs the flow. The contribution of incidence effects becomes apparent at medium frequencies and can be explained by defining an effective angle of attack. The maximum downforce is obtained at high effective angles of attack. As the frequency is increased even further, the only apparent effect is that of added mass. In this regime, downforce is shown to be related to the vertical acceleration of the airfoil. These mechanisms are independent of Reynolds number.

Nomenclature

a	=	heaving amplitude
C_D	=	drag coefficient
C_L	=	lift coefficient
C_p	=	pressure coefficient
c	=	airfoil chord
d_t	=	maximum thickness
f	=	heaving frequency
h	=	airfoil ride height
$\hat{h}$	=	nondimensional airfoil displacement, $2(h - h_0)/a$
$h_{\max}$	=	maximum ride height
$h_{\min}$	=	minimum ride height
h_0	=	mean ride height
k	=	reduced frequency, $\pi f c/U_\infty$
L	=	downforce, positive down
L_{mass}	=	downforce due to added mass effect
Re	=	Reynolds number based on wing chord c, $\rho U_\infty c/\mu$
T	=	heaving period, f^{-1}
t	=	time
U	=	velocity magnitude
U_∞	=	freestream velocity
u	=	streamwise velocity component
v	=	heaving velocity, $\mathrm{d}h/\mathrm{d}t$
x, y	=	Cartesian coordinates, x positive downstream, y positive up
x_s	=	separation point along the chord length
y^+	=	nondimensional normal wall distance
α_0	=	airfoil incidence
α_{eff}	=	effective airfoil incidence
ϑ	=	volume of fluid
ρ	=	density
τ	=	nondimensional time, t/T
φ	=	phase lag
ω	=	vorticity, $\partial v/\partial x - \partial u/\partial y$

Received 1 December 2009; revision received 7 October 2010; accepted for publication 24 January 2011.

*Ph.D. Student, School of Engineering Sciences.
†Professor, School of Engineering Sciences. Associated Fellow AIAA.

I. Introduction

WINGS in ground effect and oscillating wings are two interesting and well-known subjects, but they have rarely been studied together. The field of wings in ground effect deals with wings placed in close proximity to the ground, particularly when the ground moves at the freestream velocity, as is the case of racing cars. It has been reasonably covered and there seems to be a general understanding of the aerodynamics. As the available resources have increased, dynamic testing has become more attractive. However, racing cars are seldom in a steady state. An understanding of the dynamic behavior of the wing can help a driver control the car, as well as in the design and setup of the car. In the cases where adjustable flap angles are allowed, the performance through the corners can increase dramatically. Regarding oscillating wings, most of the studies have focused on insect flight and micro air vehicles (MAVs) [1–3]. Insects fly at low Reynolds numbers, so the flow physics differ from racing car wings. Furthermore, both applications are generally focused on thrust generation and wake structure. While previous works have managed to acknowledge the configuration of the wake and forces as a function of the main parameters, they miss the fundamental reasons behind this variation. In the case of an oscillating wing in ground effect, it would be impossible to discern the important phenomena acting at low frequencies with a simple study of the flow contours. Regarding the application to race cars, where decisions have to be made quickly, a driver needs a predictable car so that he can be aware of what will happen next and, most important, when it will happen. Therefore, an investigation of the instantaneous force distribution over time might provide a better answer than previous approaches. It is these reasons that motivate this study of a heaving airfoil in ground effect. It will be shown that the flow physics can be described by means of three mechanisms: as well as the effective incidence and added mass effects observed in freestream and highlighted by Theodorsen's linear theory [4], the ground effect plays an important role in the presence of a moving plane. There are no previous studies on the relative influence of each mechanism for an airfoil in ground effect. The contribution of each of the mechanisms to the aerodynamic performance of the airfoil will depend on the frequency of oscillation and the distance to the ground. Indeed, in freestream added mass effects take over incidence effects at high frequencies [4,5], but this has not been proven for an airfoil in ground effect. Furthermore, the effect of the ground on a stationary airfoil depends on the height of the airfoil [6], so it was postulated that the relative contribution of the ground effect to an oscillating airfoil depends on both the frequency and the ground clearance. The use of a downforce-generating airfoil is suitable for race car applications, although the results could be extrapolated to insects and MAVs flying

close to the ground. The effect of freestream velocity on the performance of the oscillating airfoil might be of interest in some cases and is presented as an appendix.

Many experimental and computational studies have been performed on wings in ground effect for general aeronautical purposes, but it has not been, since the last 10 years that studies on race car wing have been presented. Dominy [7] stated that the effect of the ground on a downforce-generating wing is to increase the suction on the lower surface. Close to the ground, stall occurs due to the adverse pressure gradient on the suction surface. Zerihan and Zhang [6,8] and Zhang and Zerihan [9,10] performed several detailed investigations on wings in ground effect. Experimental tests in a wind tunnel equipped with a moving ground facility, including force measurements, surface pressures, and flow visualization techniques, showed that as the ground is approached, downforce first increases in a force enhancement region, then there is an enhancement slowdown until, below around $0.1c$, the wing stalls and downforce drops. The force reduction phenomenon was shown to be due to separation of the boundary layer. Separation occurs due to the adverse pressure gradient and not due to the boundary layers merging. The downforce curve shape changes with ride height, its slope increasing with ground proximity. Fixing the transition point had an adverse effect, reducing the downforce and increasing the maximum downforce height. Computational studies were also available in order to compare to the experiments. The performance is well predicted except the wake downstream of the wing, which is predicted to be thicker than the measurements. In addition, the ground boundary-layer thickness is overpredicted using a two equation turbulent model. Finally, measurements off surface using laser Doppler anemometry and particle image velocimetry showed that the size of the wake increases in proximity to the ground, with a downward shift of its path. An edge vortex is formed on the edge of the endplate of the wing, contributing to the force enhancement. The enhancement slowdown is partly due to the vortex breakdown and the maximum downforce is found at the height where the vortex breaks down completely and stalls appear. The force reduction region covers ride heights below the breakdown.

Earlier attempts to analytically resolve the forces on oscillating airfoils correspond to Theodorsen [4] and Garrick [11]. For an airfoil under small amplitude oscillations and assuming potential flow, Theodorsen [4] proposed a linear theory to determine the lift generated by a plunging and pitching airfoil. Garrick [11] extended Theodorsen's theory to account for the drag or propulsive force. Despite their applicability to inviscid flows only, the resulting expressions are still valid to analyze trends or phase shifts between forces and motion. In 1934, von Kármán and Burgess [12] showed that a jetlike vortex pattern was formed behind a flat plate in oscillatory motion, although the effect of thrust production by an oscillating airfoil is known as the Knoller–Betz effect, since it was Knoller [13] and Betz [14], independently, who discovered that an airfoil moving vertically generates an effective angle of attack, which results in a force vector tilted forward. Von Kármán and Burgess [12] identified the physical phenomena related to this behavior. They showed that a reverse vortex sheet develops behind the body, as opposed to drag-producing wakes.

The wakes of oscillating airfoils can be split into three groups: drag-generating, neutral and thrust-generating wakes. Drag-generating wakes are characterized by a Kármán vortex street, while a reverse Kármán vortex street is typical of thrust-generating wakes. For drag-producing wakes, time-averaged velocity profiles of the wake will show a momentum deficit similar to a stationary airfoil. Thrust-producing wakes will have a jetlike time-averaged velocity profile. It was acknowledged by Freymuth [15] that airfoils can generate thrust due to a reverse von Kármán street being formed in the wake. The structure of the wake is modified by the amplitude, frequency, and pattern of oscillation, as studied by Koochesfahani [16] for a pitching airfoil at a Reynolds number $Re = 12,000$ and small amplitudes, using both flow visualization and laser measurements. The airfoil will generate thrust only above a critical frequency, and this depends on the amplitude of the oscillation. Similarly, Jones et al. [17] used flow visualization to prove that plunging airfoils generate thrust only over a certain $k \cdot a$. Their inviscid panel code compared well to the experiments, except for low values of $k \cdot a$ in which viscous effects become important. This agrees with the fact that the evolution of the wake structures is an inviscid phenomenon.

The parameters that define the wake structure are the reduced frequency k and the amplitude a, as shown by Young and Lai [18], who simulated the plunging motion of a NACA 0012 airfoil at $Re = 20,000$. The results compared well with the experiments by Lai and Platzer [19] at the same Reynolds number, under the assumption of laminar flow. Turbulent results do not agree well with experiments, indicating that either the experiments by Lai and Platzer were in laminar flow or turbulence models might not capture properly the separation and vortex shedding near the trailing edge of an unsteady airfoil. Vortex-pair shedding observed by Lai and Platzer [19] was explained by Young and Lai [20] as the result of an interaction between the natural shedding of the airfoil and the plunge frequency. Compared with the forced vortex shedding, this can only be captured by viscous methods. They defined a vortex lock-in boundary in the k–a plane in which this interaction occurs. Inside the vortex lock-in region, vortices are shed at the plunging frequency, while outside this region natural shedding dominates the wake structure. Note that these results are valid for low Reynolds numbers, in which a laminar flow assumption can be acceptable. At high enough Reynolds numbers, natural shedding physically disappears and only the flapping frequency defines the wake structure. It is then possible to have no vortex shedding at low k.

In one of the few bidisciplinary analysis, Moryossef and Levy [21] numerically studied an oscillating inverted airfoil at $Re = 4.6 \times 10^5$ close to the ground. They covered a range of ride heights inside the force enhancement region. The results show appreciable differences between viscous and inviscid simulations in terms of force quantity. Nevertheless, thrust generation was shown to be an inviscid phenomenon. For inviscid flow, the lift phase lag approaches zero when the reduced frequency approaches zero, and there is a maximum lag at $0.25 \leq k \leq 0.40$, depending on the ride height. This maximum decreases and moves to higher frequencies with decreasing ground clearance. There are no references to the phase lag in viscous flow. No results in the force reduction region were presented, region in which the difference between viscous and inviscid flow becomes more apparent in terms of flow physics.

Regarding the mechanisms that define the flow physics in this study, two of them have already been identified before. For instance, Minotti [22] exposed the reasons why steady aerodynamic measurements underestimate the forces developed by flying insects. Among those reasons, rotational circulation and inertia effects are of interest at high Reynolds numbers. Rotational circulation refers to the increase in lift when the angle of attack increases with time. Inertia effects are associated with the acceleration of the wing and are particularly important when the rotational velocity changes and near stroke reversal.

On a similar note, Andro and Jacquin [5] proposed three mechanisms acting on a heaving airfoil, based on direct numerical simulations at $Re = 1000$. These are leading-edge vortex shedding, added mass reaction, and wake capture. While added mass reaction is apparent only at high frequencies, at low frequencies there is a quasi-steady regime in which the effective incidence plays an important role, together with the leading-edge vortex, which, if shed, could lead to stall. Leading-edge vortices and wake-capture effects might not be discernible at high Reynolds numbers, in which the boundary layer remains mostly attached. Conveniently, incidence and added mass effects are clearly exposed by Theodorsen's equation. However, the influence of the moving ground, including viscous effects, is not accounted for and must be studied numerically.

II. Airfoil Geometry

A sketch of the inverted airfoil with the suction surface closer to the ground is shown in Fig. 1. The airfoil is the profile of the main element of the double-element configuration used in [23]. The chord c, distance between leading edge and trailing edge, is 139 mm.

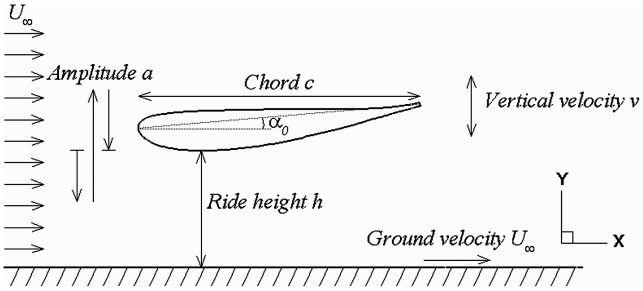

Fig. 1 Sketch of the airfoil near the ground plane, showing the definition of airfoil chord c, amplitude a, vertical velocity v, ride height h, angle of attack α_0, and freestream velocity U_∞.

Maximum thickness is $d_t/c = 0.14$. The airfoil has a finite trailing edge of $0.01c$. The incidence α, defined as the angle between the chord and the horizontal plane, was set to 5°. Incidence is taken as positive when the leading edge is lower than the trailing edge. The ride height or vertical distance from the ground h is defined as the distance from the lowest point on the suction surface to the ground. Whereas the incidence remained constant, the ride height changed with time during the simulation.

The axes were orientated such that x was aligned with the incoming flow and positive downstream, and y was normal to the ground and positive upward. For nomenclature purposes downforce, or negative lift, is considered positive when pointing to the ground.

III. Numerical Method

The airfoil was tested within the FLUENT 6.3 unsteady Reynolds-averaged Navier–Stokes solver. The equations were solved using an incompressible pressure-based solver, double-precision, second-order accurate in space and SIMPLEC coupling.

Implicit time integration was used, with 30 subiterations per time step. Only first-order discretization of the unsteady terms was available for dynamic meshes. By using a different approach, which involves moving the reference frame and adding an additional source term to the momentum equations, second-order time discretization could be tested for an airfoil in freestream. There were no changes to the flowfield at the specified time step with respect to first-order discretization. Because of the presence of the ground, this approach could not be used for the airfoil in ground effect. Nevertheless, a time refinement study, together with the comparison in freestream, leads to the conclusion that first-order results could be trusted to a certain extent. The nondimensional time step varied from $\Delta\tau = 1 \times 10^{-4}$ to 1×10^{-3}, depending on the frequency. As the frequency decreased, $\Delta\tau$ was reduced to ensure a not-too-high physical time step such that the unsteady phenomena could be properly captured.

For the main part of this study, the simulations were performed at a constant Reynolds number Re of 3.9×10^5, based on the chord of the airfoil. By manually adjusting the turbulence levels at the inlet and outlet, the high turbulence of the freestream flow ensured that the flow was turbulent through the entire airfoil surface. After a comparison of different turbulence models, a one-equation Spalart–Allmaras (S-A) model [24] was chosen as the best compromise between accuracy and expense. The S-A model gave similar results to the two-equation realizable κ-ε and shear stress transport κ-ω models in terms of pressure distribution and unsteady forces. The low-quality standard κ-ε and standard κ-ω models predicted much lower suction, lower downforce, and higher drag, whereas the renormalization group κ-ε model was closer to the first group, but overpredicted the drag. These results show a similar trend to stationary simulations. Indeed, at this Reynolds number, the S-A model has been previously chosen as the optimum turbulence model to simulate airfoils [25] and cylinders [26] in ground effect with great accuracy. The comparisons to experiments proved more successful than other models, particularly in the wake and in the channel between airfoil and ground. Although the previous studies focused on stationary bodies, their conclusions are still valid for low frequencies, in which the flow is quasi-stationary. Furthermore, the turbulence models seem to perform similarly in the stationary and the oscillatory cases, so the results of the first group of models will be more reliable than the rest. Among these, the one-equation S-A model will be faster. Outside the quasi-stationary range, the flow becomes increasingly inviscid and the turbulence model is no longer relevant. The Mach number was $Ma = 0.12$, low enough to assume incompressible flow.

For the inviscid simulations, an inviscid model available within the solver was used. The other parameters were not altered.

The unsteady simulations were started from a uniform flowfield with freestream conditions in the entire domain. The flow undergoes an initial transient during the first few periods of oscillation, until the flow stabilizes and a periodic solution is obtained. The time to reach this state depends on the frequency of oscillation. The results shown in this study correspond to the periodic solution.

A. Heaving Motion

The heaving motion is sinusoidal and of amplitude a and frequency f, as seen in Fig. 2, so if the airfoil is initially at the mean position $h = h_0$, then

$$h(t) = h_0 - \tfrac{a}{2}\sin(2\pi f t) \tag{1}$$

A nondimensional form of the vertical displacement is

$$\hat{h}(\tau) = -\sin(2\pi\tau) \tag{2}$$

Using a dynamic mesh model, the grid was adapted after each time step. The surrounding domain was moved simultaneously to avoid undesired skewness and mesh deformation near the airfoil, so that restructuring of the grid occurred at a distance far enough from the airfoil to ensure that the results were not influenced by it.

It is also possible to nondimensionalize the frequency, obtaining a reduced frequency:

$$k = \frac{\pi f c}{U_\infty} \tag{3}$$

Once the Reynolds number is fixed, the problem reduces to imposing the values of k and the amplitude of the heaving motion a. In this study $a/c = 0.08$, therefore the heaving motion depends on only one parameter, k. Physically, the reduced frequency represents the ratio between the length of the bound vortex sheet, equal to the chord c, and the length of the vortex sheet shed during one cycle of oscillation, U/f. Hence, the reduced frequency is a representation of the interference effect between the bound vortices and the shed vortices [27].

B. Grid Structure

A hybrid grid was created to resolve the flow around the airfoil (Fig. 3). Ideally, accuracy is improved by using a structured mesh, but

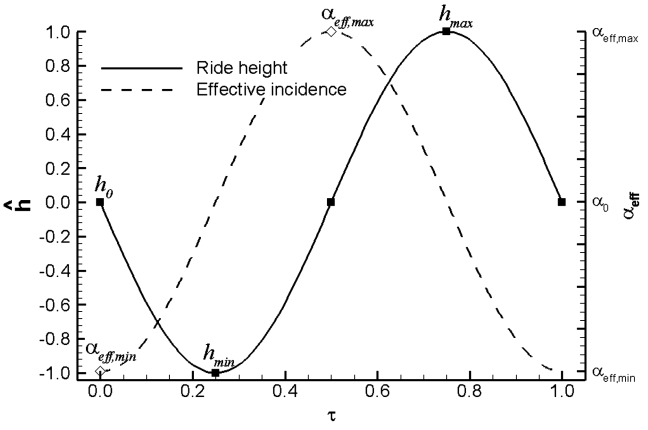

Fig. 2 Sketch showing a sample sinusoidal motion of the airfoil and the corresponding variation of effective incidence.

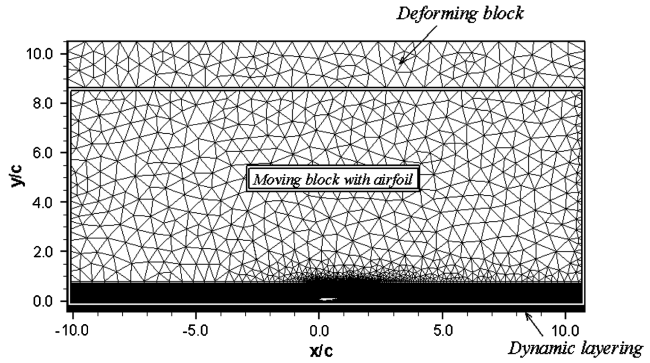

Fig. 3 Illustration of the domain and mesh, showing the block structure.

the main drawback is that it is not suitable for deforming domains, where cells have to be created, destroyed and stretched. This makes unstructured meshes ideal for this case. However, the study of an airfoil requires the use of boundary layers and structured elements that follow the shape of the contour so that common features like gradients, separation, vortex shedding and wake can be adequately captured. In addition, it is important to resolve the flow between the airfoil and the ground. Taking into consideration the advantages and drawbacks of both methods, we opted to divide the domain into three horizontal blocks that extend from inlet to outlet: an upper unstructured block far away from the airfoil; a middle block split into a structured region containing the airfoil and extending $0.72c$ above it plus an unstructured region above it; and a bottom structured block that includes the ground boundary layer. Note that although the ground moves at the freestream velocity there is a higher-velocity channel between airfoil and ground, making the use of a refined mesh imperative to capture the boundary layer on the ground. The middle block moves with the airfoil so that the mesh around the airfoil does not deform at any point. The elements in the upper block are deformed in a manner that resembles springs, but the deformation is relatively small compared with the actual displacement of the boundary. Special attention was paid to the boundary between the middle and the bottom blocks, to ensure continuity in cell size as the airfoil oscillates. This is important, since structured layers are created or destroyed in the ground block, depending on the size of the neighboring layer. The mesh around the airfoil and boundary layer is C-shaped.

An independence study determined the appropriate dimensions for the domain. The top wall was modeled as a symmetry plane and was placed $10.5c$ above the airfoil. The grid extended $10c$ upstream of the leading edge of the airfoil onto a velocity inlet and $10c$ downstream of the trailing edge onto a pressure outlet. The velocity on the ground was set equal to freestream to simulate a moving ground plane.

A mesh refinement study was undertaken under both stationary and heaving conditions. Results presented in this study are based on a 151,000-point grid, for which convergence of the force coefficients was achieved and the wake region was sufficiently refined to capture the unsteady phenomena. The airfoil surface contains 505 points and the boundary-layer block 30 points, the initial cell spacing normal to surface being $1 \times 10^{-4}c$. This gives a $y^+ \approx 1$. Maximum skewness was limited to an equi-angle[‡] of 0.55, while the average was 0.08.

For the simulation of the airfoil in freestream, the bottom block was extended vertically with unstructured elements down to a distance similar to the upper block and the moving ground condition was replaced by a symmetry plane. For the inviscid simulations, the boundary-layer block was reduced to 10 normal elements and an initial spacing of $7 \times 10^{-4}c$. The boundary condition at the ground was changed to a stationary wall.

[‡]Computed as $\max[(Q_{\max} - 90)/90, (90 - Q_{\min})/90]$, where $Q_{\max}$ and $Q_{\min}$ are the largest and smallest angle (in degrees) in the cell, respectively. A value lower than 0.8 is generally considered acceptable.

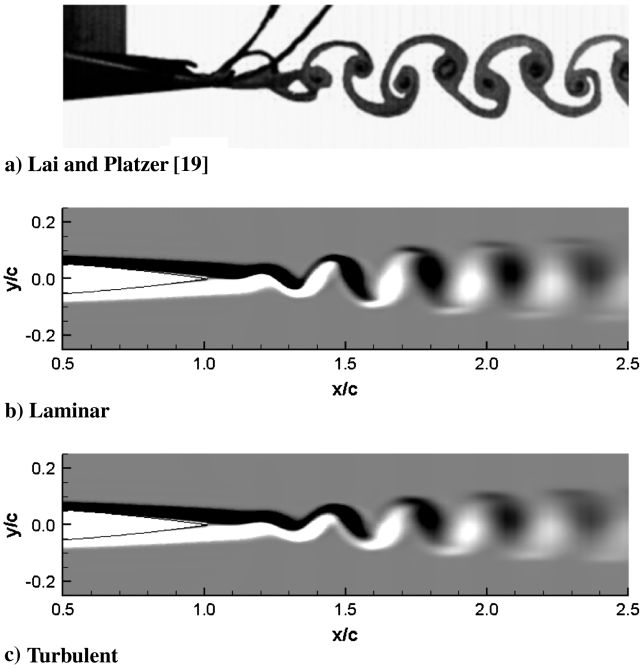

a) Lai and Platzer [19]

b) Laminar

c) Turbulent

Fig. 4 Vortex shedding behind a stationary NACA 0012 airfoil at $Re = 20,000$.

IV. Method Validation

The numerical method was validated by using a NACA 0012 airfoil at $Re = 12,000$ and 20,000. Both laminar and turbulent simulations were in good agreement with previous experiments. At $Re = 12,000$, a natural shedding frequency k_{nat} of 8.45 was predicted, which compares favorably with $k_{\text{nat}} = 8.71$ as determined experimentally by Koochesfahani [16] under similar conditions. At $Re = 20,000$, k_{nat} is 10.65 for the laminar case and 10.35 for the turbulent case, whereas Young and Lai [20] numerically measured a value of 9.4. The vorticity contours for both cases and for the experiments undertaken by Lai and Platzer [19] at the same Reynolds number are shown in Fig. 4. The shedding process is properly simulated, albeit with a slight diffusion of the vortex cores. The flow separates at $x/c = 0.75$, resulting in an effective blunt trailing edge. Shedding occurs in the form of a Kármán vortex street, similarly to bluff bodies.

Simulations of the inverted airfoil at $Re = 20,000$ show that this particular airfoil does not naturally produce vortex shedding. Instead, a shear layer is formed on each side of the trailing edge. As a matter of fact, the flow separates on the suction surface, but not on the pressure surface, so that there is not an effective symmetry that could lead to instabilities. It is obvious that the inability of this airfoil to produce natural shedding is due to its characteristics and not as a result of the specific code. In any case, the following results are for $Re = 3.9 \times 10^5$ and high-turbulence flow, in which case it would be more difficult to find natural vortex shedding in the wake.

V. Results

A. Stationary Airfoil

The dependence of the downforce coefficient with ride height is presented in Fig. 5. These results are in qualitative agreement with Zerihan and Zhang's [8] experiments for an inverted airfoil in ground effect. Based on the different aerodynamic phenomena observed for the stationary airfoil four regions were selected to study the oscillating airfoil.

1) Region 0 is in the freestream. Out of ground effect there is only one possible result. This serves as a reference case. The downforce and drag coefficients are $C_L = 0.98$ and $C_D = 0.022$, respectively.

2) Region 1 is in the force enhancement region. The airfoil was placed inside the region of increasing downforce with ground proximity, but the forces are relatively small and the rate of increase

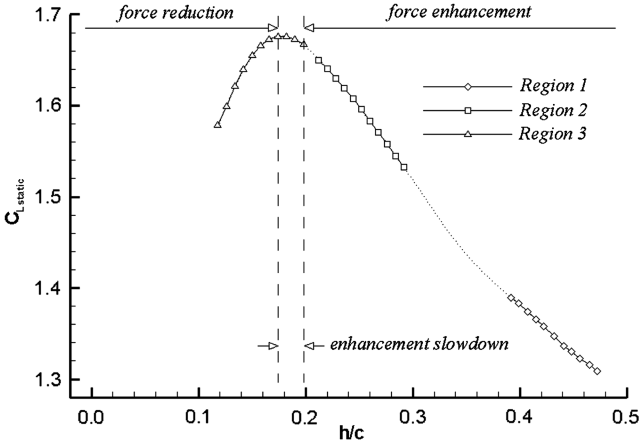

Fig. 5 Variation of downforce coefficient ride height for a stationary airfoil.

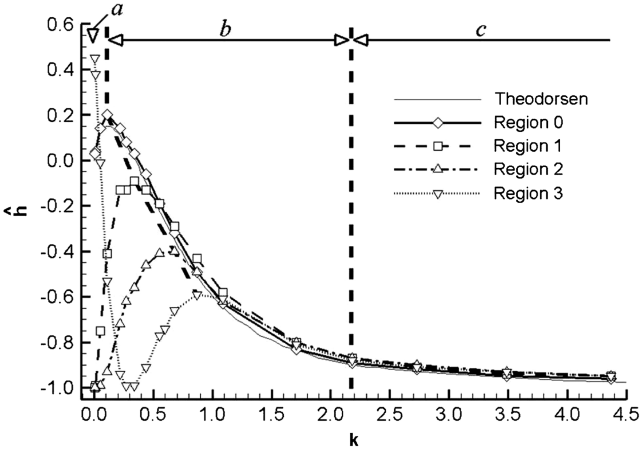

Fig. 6 Variation of position of the maximum downforce with reduced frequency for all regions. The boundaries between regimes are traced by thick dashed lines.

of downforce is low. In this region, downforce increases with ground proximity in a linear fashion. Downforce increases because the flow increasingly accelerates in the region between the airfoil and the ground and results in greater suction on the lower surface. The effect of the ground is appreciable, although not as strong as in region 2. The downforce coefficient is in the range between $C_L = 1.30$ and 1.39, which is an increase of 33–42% with respect to freestream. Drag also increases with decreasing ride height, $C_D = 0.029$–0.031, which is 32–41% higher than in freestream.

3) Region 2 is in the force enhancement region. The airfoil is close to maximum downforce and the rate of increase of downforce with ground proximity is maximum. The airfoil is close to the force enhancement slowdown region, since the slope of the curve starts to decrease toward the lowest ride heights, due to the onset of separation of the boundary layer as the adverse pressure gradient increases on the suction surface. The downforce coefficient is in the range between $C_L = 1.53$ and 1.65, which is an increase of 56–68% with respect to freestream. Drag increases with decreasing ride height, $C_D = 0.036$–0.045, which is 63–103% higher than in freestream.

4) Region 3 is in the force enhancement slowdown and force reduction region. The rate of increase of downforce decreases and, as a consequence, downforce reaches a maximum of $C_L = 1.68$ at $h/c = 0.17$ and then decreases. This maximum represents an increase of 71% with respect to freestream. The loss in downforce is due to excessive separation on the suction surface [8]. On the other hand, drag increases with ground proximity, $C_D = 0.048$–0.073, which is 113–227% higher than in freestream.

The respective ride height ranges are collated in Table 1.

B. Oscillating Airfoil

Since there is no natural shedding, the only characteristic frequency is that of the vertical motion. An analysis of the instantaneous forces on the airfoil, namely, downforce and drag, shows that they exhibit a periodic behavior with the same frequency as the airfoil. They can be approximated by a sinusoidal function with sufficient accuracy. However, the curves that represent the vertical motion with time are out of phase with the force history, and this phase lag varies with reduced frequency. For a better understanding of the lag, one can choose to study one characteristic point in the cycle instead of the actual phase lag (which is not very intuitive). For that reason in this study the parameter taken is the maximum in the downforce curve. The value of the independent variable at this point (τ) changes with frequency, such that a new chart can be compiled: position of maximum downforce against reduced frequency in each region. The study of this phase lag can provide some useful insight into the physics of the flow, as it is a true indicator of the main causes that produce the forces. Although different phenomena take part at the same time in the configuration of the flow around the airfoil, it is possible to isolate the effect of each of them through this analysis.

Table 1 Characteristic ride heights in each region (static stall at $h/c = 0.17$)

Region	h_{max}/c	h_0/c	h_{min}/c
0	——	——	——
1	0.47	0.43	0.39
2	0.29	0.25	0.21
3	0.20	0.16	0.12

Figure 6 presents the alternative phase lag curves for each region. There are three clearly defined regimes (a, b, c). Considering that a phase lag of zero corresponds to the maximum downforce occurring at the bottom position, then in regime a the phase lag increases up to a maximum lag that depends on the region. Although the position of maximum downforce initially decreases in region 3, this occurs during the downstroke, so the downforce leads the motion. The phase lag is in fact increasing and once it reaches zero, the downforce lags the motion. In the other regions, the downforce always lags the motion (i.e., the maximum occurs during the upstroke). In regime b, the phase lag decreases and is independent of the region for $k \geq 1.09$. In regime c, the curves are identical and reasonably constant.

An additional curve representing the phase lag according to Theodorsen's theory is shown in Fig. 6. Theodorsen [4] developed an analytical expression for the lift generated by an airfoil under sinusoidal motion. Although the solution is restricted to a symmetric airfoil in freestream and potential flow for small oscillations, it is still valid in region 0 where viscous effects are not important.

Accounting for our own sign convention, the expression for the downforce can be written as follows:

$$L = \underbrace{\tfrac{1}{4}\pi\rho c^2 \ddot{y}}_{\text{noncirc}} + \underbrace{\pi\rho U_\infty c C(k)\dot{y}}_{\text{circ}} \tag{4}$$

where $C(k) = F(k) + iG(k)$ is a complex function, known as Theodorsen's function [4,28]. The effect of $C(k)$ is to introduce a phase shift in the circulatory part of the aerodynamic load. This phase is initially zero; thus, the phase lag is caused by the vertical velocity vector, which is 90° out of phase with the motion. Then $\hat{h} = 0$ in the phase lag diagram. The phase shift due to $C(k)$ increases quickly with frequency. The maximum negative phase of $C(k)$ occurs at $k \approx 0.2$, which corresponds to the maximum phase lag in region 0. It then asymptotically tends toward zero again, but in this case the phase lag is dominated by the noncirculatory term, proportional to the acceleration and the frequency squared. The downforce is in phase with the motion (according to our definition of phase lag) and $\hat{h} \to 1$ in the phase lag diagram.

Making use of complex algebra, it is possible to analytically obtain the expression for the phase lag by using $y = ae^{i\omega t}$:

$$L = 2\pi\rho U_\infty^2 \left[-\frac{k^2}{2} - Gk + iFk \right] a e^{i2\pi ft} \tag{5}$$

$$L = 2\pi\rho U_\infty^2 \left\{ -\frac{k^2}{2} - Gk + iFk \right\} y \tag{6}$$

The phase lag with respect to the motion is

$$\phi = \arctan\left(-\frac{F}{\frac{k}{2} + G} \right) \tag{7}$$

Note that there are three different solutions to Eq. (7). The correct one has to agree with the sign convention: a phase lag of zero corresponds to maximum downforce at the bottom position. In freestream, downforce always lags the motion by less than half a period so $-180° < \varphi < 0°$. To plot the analytical solution, it is necessary to convert the phase lag into a vertical position:

$$\hat{h} = -\cos\phi \tag{8}$$

The values of F and G are tabulated and can be found in many sources (e.g., [28]). As shown in Fig. 6, the correlation between the analytical solution and the numerical solution in region 0 is excellent. Furthermore, since all the curves collapse into one in regime c, the physics in that regime can be predicted by Theodorsen's solution for any ground clearance. Moreover, the solution at higher k can also be deduced as only the noncirculatory term prevails.

The existence of three regimes is directly linked to three mechanisms that govern the flow. Two of them appear in Theodorsen's theory: the noncirculatory part represents the effect of added mass and the circulatory part represents the effect of vorticity in the flow and is proportional to the effective incidence caused by the vertical motion. The third feature is the ground effect, which plays an important role in regions 1, 2, and 3. A detailed analysis of the influence of each effect on the phase lag is presented in the following sections.

1. *Ground Effect*

If the heaving motion is relatively slow, the flow, for realistically large time steps, will be constantly in equilibrium and might be compared with the stationary case at each position. The first question one might be interested in answering is at which frequencies the flow can be considered quasi-stationary. The results show that for reduced frequencies up to $k = 0.01$ the differences between the heaving and the stationary airfoil are negligible. For the next lowest frequency, $k = 0.05$, the first differences appear not so much at the top and bottom positions where the vertical velocity is zero and around which the airfoil moves slowly, thus discarding dynamic effects, but near the mean position where the velocity of the airfoil is at a maximum. Whereas at the extreme positions it remains fixed, at the mean position the separation point changes and the forces change too. For $k > 0.11$ the flow is no longer quasi-stationary at any point.

It must be noted that there is a parallelism between ground proximity and incidence on a stationary airfoil. When the incidence increases, more suction is generated on the suction surface and, as a consequence, more downforce. But at high angles the adverse pressure gradient becomes too high and the boundary layer starts to separate. Downforce might continue to increase up to point where separation is massive and the airfoil stalls (obviously the separation process depends on the particular airfoil, but this serves as a generic explanation). Similarly, an inverted airfoil getting closer to the ground will experience the same events. Initially downforce increases due to a venturi channel being created between the lower surface and the ground, which results in higher velocities and lower pressure in the channel. At the same time the flow has to recover the pressure along the lower surface to fulfill the Kutta condition at the trailing edge. Since the suction peak becomes stronger with ground proximity, the pressure recovery will also be bigger, so an adverse pressure gradient will develop downstream of the suction peak. At very low ride heights this gradient will become unsustainable for the attached flow and it will separate from the surface of the airfoil. When the negative contribution of this separation to the downforce becomes more important than the gain from the increasing suction the airfoil will stall. This particular airfoil does not presents separation in region 1, but the flow starts to separate in region 2. This may also be seen in the isoline of $u = 0$ in Fig. 7 for $k = 0.01$. The drop-off in downforce for the stationary case starts at $h/c = 0.17$ ($\hat{h} = 0.40$, region 3), for which case the separation point is at $x_s/c = 0.73$.

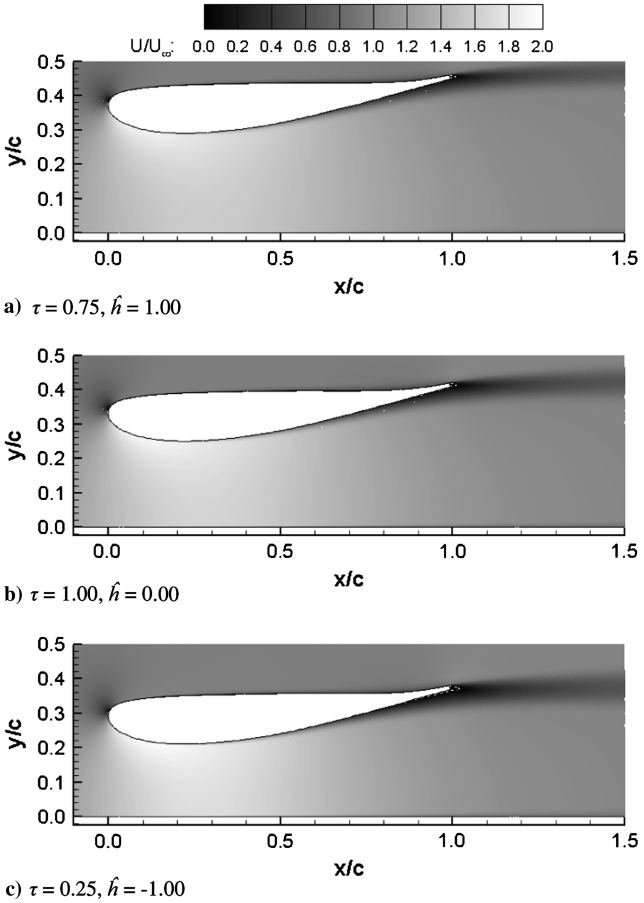

Fig. 7 Contours of nondimensional velocity in region 2 at $k = 0.01$. Dashed lines denote isolines of $u = 0$.

The main consequence of this quasi-stationary behavior is that the ground effect will govern the aerodynamic performance of the airfoil. This means that the maximum downforce will occur at or very near to the bottom position in regions 1 and 2, as shown in the phase lag curves in Fig. 6 for $k \to 0$, and near $\hat{h} = 0.40$ in region 3, which corresponds to the ride height of the maximum downforce for the stationary airfoil. For lower ride heights, the venturi effect cannot overcome the effect of separation, seen in Fig. 8, and the airfoil stalls.

2. *Incidence Effect*

The second mechanism that influences the flow is the effective angle of attack. From the point of view of the airfoil, the heaving motion and the pitching motion are similar, since in both cases the airfoil sees two incoming velocities: the freestream velocity U_∞ and the vertical velocity v. As sketched in Fig. 9, this results in the freestream flow approaching the airfoil at an angle of attack different from the original incidence. The vertical velocity is a function of the physical time, therefore the effective angle of attack is also dependent on time. Thus, there is a direct link between the effective incidence of

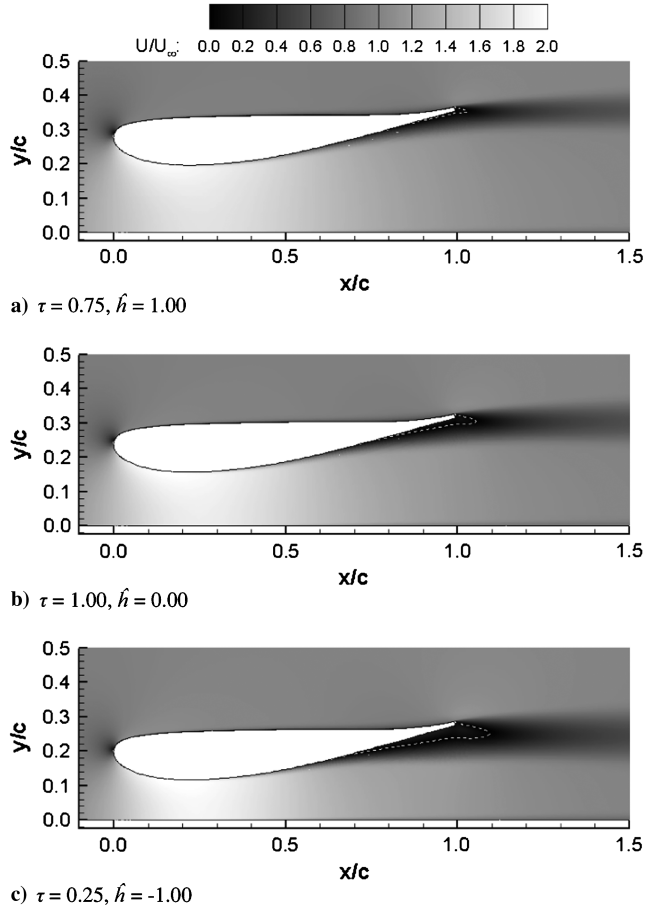

a) $\tau = 0.75$, $\hat{h} = 1.00$

b) $\tau = 1.00$, $\hat{h} = 0.00$

c) $\tau = 0.25$, $\hat{h} = -1.00$

Fig. 8 Contours of nondimensional velocity in region 3 at $k = 0.01$. Dashed lines denote isolines of $u = 0$.

a heaving airfoil and the angle of attack of a pitching airfoil. The effective angle of attack α_{eff} is given by the sum of the freestream and vertical velocity vectors:

$$\alpha_{\text{eff}}(t) = \alpha_0 + \arctan\frac{\mathrm{d}h/\mathrm{d}t}{U_\infty} \tag{9}$$

Note that according to Fig. 2, h lags α_{eff} by a quarter of a period, so that $\alpha_{\text{eff}} = 0$ at the extreme positions and $\alpha_{\text{eff,max}}$ occurs when the vertical velocity is maximum, at midupstroke.

a. Influence of Effective Incidence on Separation Caused by Ground Proximity. It has been previously discussed that the point of flow separation along the suction surface changes with respect to the stationary case. For the latter, the source of separation is the adverse pressure gradient created due to ground proximity. But when the airfoil flaps at a certain frequency, there are additional effects that modify the configuration of the boundary layer. In regions 2 and 3, where separation is appreciable, the separation point at each ride height changes with reduced frequency. For $k \leq 1.09$, a consistent pattern can be observed: for instance, at the mean position during the upstroke the separation point moves upstream with increasing frequency. And at that position the airfoil reaches the maximum effective angle of attack. In addition, the value of $\alpha_{\text{eff,max}}$ increases with frequency, since the vertical velocity increases too. A higher angle of attack promotes separation. Therefore, even small increases in α_{eff}, as is the case at low frequencies, will push the separation point further upstream. On the other hand, in regions 0 and 1 there is no separation either in the stationary or in the oscillating cases. This is because the increase in α_{eff} with frequency is not enough to purely produce separation due to incidence. For $k = 1.09$, $\alpha_{\text{eff,max}} = 10°$, which seems not to be large enough for the boundary layer to separate. But once the boundary layer has separated (regions 2 and 3), small changes in α_{eff} alter the separation point. Therefore, the effect of incidence is modified by ground proximity, leading to variable separation throughout the stroke and for different frequencies.

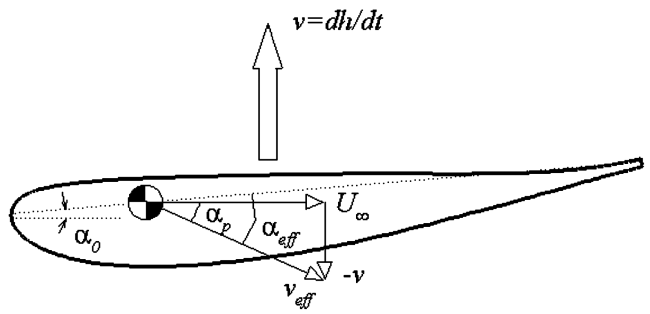

Fig. 9 Illustration of the velocities and angles as seen by the airfoil during the upstroke.

b. Regime a in Region 1. The previous remarks emphasize the fact that the effective incidence plays an important role in heaving motion. However, it will be shown that the role of incidence depends on the region and that explains why the phase lag curves differ from each other. To quantify the effect of incidence at different mean ride heights, it is necessary to study the phase lag again (Fig. 6). In region 1, $\hat{h}_{Cl\max}$ progressively moves up with increased frequency (regime a) until the maximum lag occurs for $k = 0.34$ at $\hat{h} = -0.09$, during the upstroke, just before reaching h_0. So $\hat{h}_{Cl\max}$ moves toward the point of $\alpha_{\text{eff,max}}$, which occurs at $\hat{h} = 0.00$. Therefore, incidence forces become dominant over ground effect as the frequency increases, up to $k = 0.34$. The downforce curve pattern is completely defined by the incidence angle and ground effect is almost negligible. Of course, the effect of the ground is still noticeable in the force magnitude, such that it varies among different regions, but it is the incidence effect that defines the flow configuration.

c. Regime a in Region 0. This switch from ground-effect-dominating to incidence-effect-dominating is characteristic of an airfoil in close proximity to the ground at low-medium frequencies, the incidence effect being maximum at the boundary between regimes a and b. For an airfoil out of ground effect, as in region 0, the first mechanism does not exist and $\hat{h}_{Cl\max}$ occurs near the maximum incidence for this range of frequencies. The curve does not tend to $h_{\min}$ as the frequency is reduced, since there is no ground effect. Note that $\hat{h}_{Cl\max}$ is not exactly at the mean position, but that it increases up to a maximum height and then decreases. This deviation from the mean position is caused by the unsteady factor $C(k)$ that multiplies the term due to effective incidence in Theodorsen's equation.

d. Regime a in Region 2. The theory of transition from one effect to another can be extended, with some peculiarities, to lower ride heights. Indeed, viscous effects become important and influence the result. In region 2, the phase lag curve also presents an increase from $\hat{h}_{Cl\max} = -1.00$ to a maximum, but several differences can be noted with respect to region 1. First of all, the maximum in the curve is displaced to a higher frequency ($k = 0.68$). Second, that maximum is not in the region of $\hat{h} \approx 0$.

Regarding the latter difference, a plausible cause can be attributed to the relative contribution of ground and incidence effects. The magnitude of downforce in region 2 is always greater than in region 1, so ground effect is stronger in the former region. As a consequence, the incidence effect will not be completely dominant and $\hat{h}_{Cl\max}$ will never reach the mean position (i.e., maximum incidence). Nonetheless, the incidence effect is important, as can be seen at low-medium frequencies when the maximum downforce moves from $\hat{h} = -1.00$ (ground effect dominance) to a maximum of $\hat{h} = -0.40$ at $k = 0.68$.

Of further interest is the effect of flow separation in region 2. As mentioned earlier, the high α_{eff} near the mean position combined with the ground proximity will lead to even more separation than in the stationary simulations. Thus, the maximum downforce will occur at a lower α_{eff} (earlier in the cycle than in region 1) and at a higher frequency, where viscous effects diminish. This is discernible in

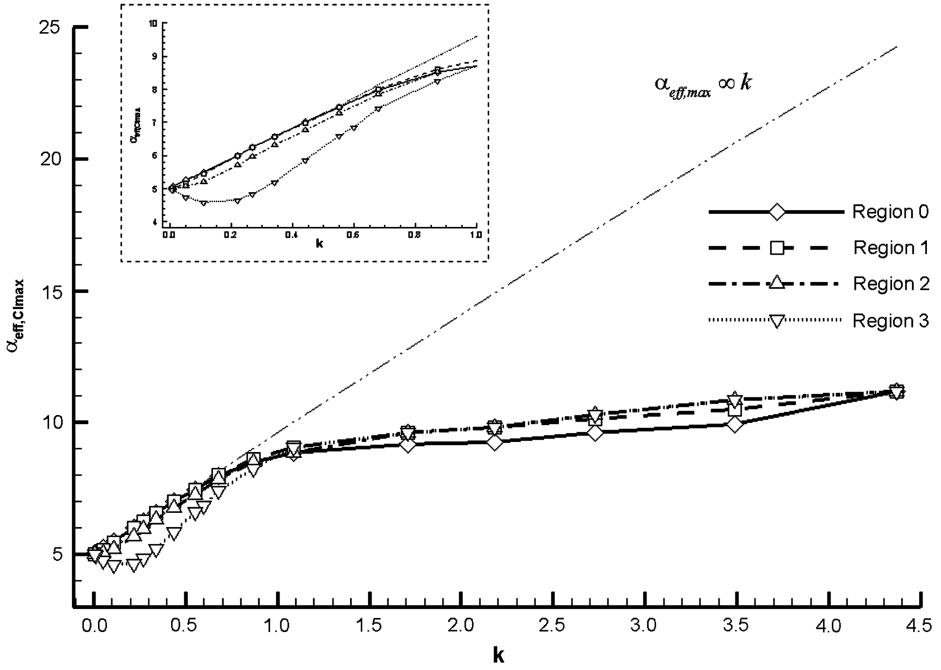

Fig. 10 Variation of effective angle of attack of maximum downforce with reduced frequency for all regions.

Fig. 10, which depicts the effective angle of attack of maximum downforce in comparison with the maximum effective angle of attack. While both match in region 0 (for $k \leq 0.55$) and region 1 (for $0.11 \leq k \leq 0.55$), the maximum effective incidence is not reached in region 2.

e. Assessment of Incidence Effect Near the Ground by Inviscid Methods. One can go even further and try to measure the relative importance of the ground against the incidence effect under the assumption that there is no separation or other undesirable viscous effects. A proper method is to use an inviscid solver, which ignores boundary layer and separation effects. In addition, downforce is overpredicted and drag underpredicted. Obviously this is physically unrealistic, yet a direct comparison to viscous simulations facilitates the identification and categorization of inviscid and viscous phenomena. Nevertheless, we must remember that these effects are not additive and it is impossible to completely isolate them by these means. A comparison between viscous and inviscid in terms of phase lag is presented in Fig. 11 for the three regions.

In the force enhancement region, or high ride heights, viscous effects are not very important, since there is no separation. The inviscid assumption would not modify the pattern of the static downforce curve, although the magnitude of the coefficients would be altered. Downforce would increase with ground proximity in a similar way to the viscous case. We have also seen that the dynamic motion does not produce separation either, so it will not be affected by the assumption of inviscid flow and the phase lag curve in region 1 can be well predicted by inviscid methods. The inviscid curve in Fig. 11a reaches a slightly higher maximum. This small difference might be due to small viscous effects that cannot be ignored.

In region 2, viscous effects are not negligible anymore. The inviscid curve in Fig. 11b follows the same pattern as the viscous one, albeit there is a divergence where the incidence effect is stronger. The maximum moves to a slightly lower frequency ($k = 0.55$ compared with $k = 0.68$) and has a greater value ($\hat{h} = -0.26$ compared with $\hat{h} = -0.40$). Nonetheless, the maximum does not reach $\hat{h} \approx 0$, for the same reason as the viscous curve: ground effect is stronger than in region 1. The displacement of the maximum toward lower values and higher frequencies with ground proximity for inviscid flow was also observed by Moryossef and Levy [21]. Hence, the two arguments used to explain the viscous curve in region 2 have been confirmed: the difference between viscous and inviscid curves reflects the influence of separation, while the difference between inviscid curves in regions 1 and 2 reflects the relative influence of ground effect with respect to incidence effect. Of course, both effects are not linear and cannot be isolated from each other, but these comparisons allow us to obtain a general idea of the concepts. Further away from the maximum the inviscid curve is expected to match the viscous curve: at low frequencies the flow is quasi-stationary and the maximum downforce will be located near the bottom position, signaling the dominance of ground effect over incidence effect. Although in this region there is flow separation, the stationary results are unaffected by this, showing increasing downforce with ground proximity.

f. Regime a in Region 3. A completely different picture can be expected from region 3. The airfoil goes through both the force enhancement and force reduction regions, meaning that static downforce decreases with ground proximity from a certain ride height. In the case of inviscid flow, downforce increases indefinitely. Under the inviscid assumption, the phase lag curve in Fig. 11c agrees with our previous comments on regions 1 and 2: the curve starts at $\hat{h} = -1.00$ and reaches a maximum at $k = 0.55$, but $\hat{h} = -0.55$, which is lower than in the previous regions. The relative influence of incidence with respect to ground effect is lower. Combined with the large separation, the maximum downforce always occurs at much lower incidences than in the previous regions (Fig. 10). In fact, in contrast to the quasi-stationary frequencies in which the maximum separation occurred at the bottom position, now separation increases with α_{eff}. The viscous curve reaches a maximum at larger frequencies, but note that at that point the flow configuration is almost inviscid, as will be explained later. The viscous curve presents a minimum at $k = 0.27$, but for $k \leq 0.27$ maximum downforce occurs during the downstroke, while for $k > 0.27$ it does during the upstroke, so the maximum is actually moving forward in the period.

As a concluding remark, the results show that the effective incidence as portrayed by Theodorsen is not only relevant in freestream, but also in proximity to the ground. However, the main difference with freestream is that incidence only becomes important at medium frequencies, when the motion is no longer quasi-stationary. Besides, reducing the mean ride height excessively leads to a lower incidence of maximum downforce due to the negative influence of early separation and to a decrease of the relative contribution of incidence effect to ground effect.

3. *Added Mass Effect*

The added mass feature can be observed at high frequencies and is related to the vertical acceleration of the airfoil. The airfoil will have

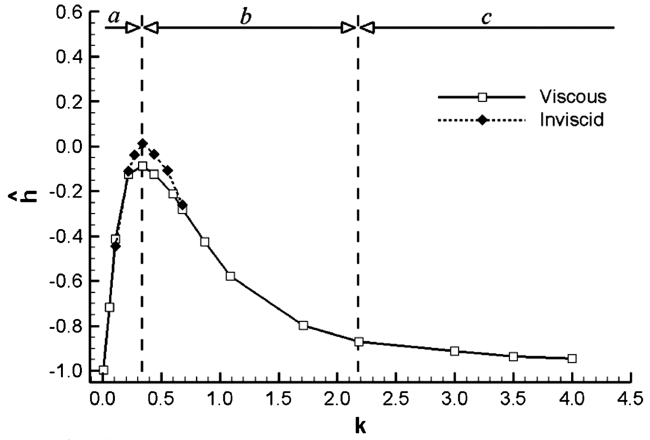

a) Region 1

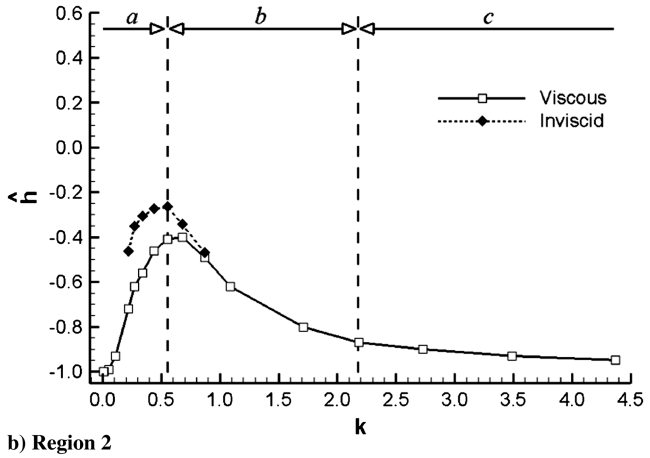

b) Region 2

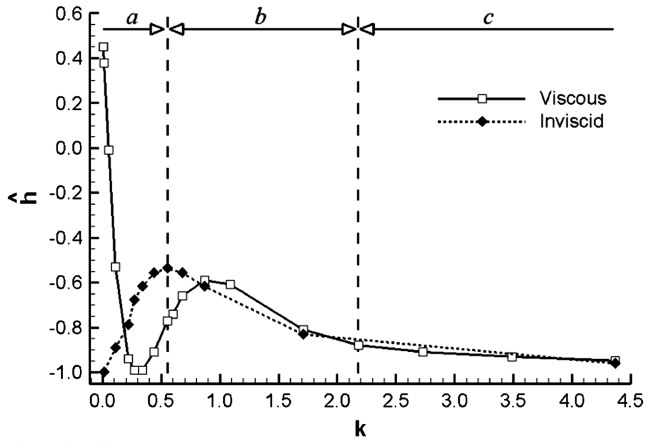

c) Region 3

Fig. 11 Variation of position of maximum downforce with reduced frequency in viscous and inviscid flow.

to displace a certain volume of fluid to occupy that space, effort that will be translated into a reaction force on the airfoil. This effect is usually neglected at low accelerations due to the density difference between body and fluid. For an airfoil that accelerates only in the vertical direction:

$$L_{\text{mass}}(t) = \rho\vartheta\frac{\mathrm{d}^2h}{\mathrm{d}t^2} \tag{10}$$

When added mass effects become important, downforce is directly proportional to the acceleration. Based on the axis orientation and the definition of downforce, a positive vertical acceleration results in positive downforce, which is to say lift pointing downward. Then the maximum downforce occurs where acceleration is at a maximum, and this happens at the beginning of the upstroke.

As shown in Fig. 6, after the maximum the phase lag curves all decrease in regime b and tend to an asymptotic value in regime c. Regardless of the region, all curves tend to $\hat{h}_{Cl\max} = -1.00$, where the added mass forces generate the largest amount of downforce. Also, the curves merge into one for $k \geq 1.01$. The first immediate conclusion is that the flow pattern is unaffected by the presence of the ground, although the magnitude of the coefficients is affected. This immediately discards the idea that ground effect could play a role in moving the location of the maximum downforce back to lower ride heights. Regime c, in which the phase lag is relatively constant with frequency, is characterized by a prevalence of added mass effects over incidence effects.

Additionally, the inviscid curves in Fig. 11 match their viscous counterparts. Added mass effects are of an inviscid nature.

The importance of an asymmetric profile and initial angle of attack is shown by the fact that in region 0, although the strokes are symmetrical, average lift is not zero. In fact, it is even greater than at low frequencies. For a symmetric airfoil at zero angle of attack, lift due to the added mass would average zero [5]. In addition to the aforementioned asymmetry, the effect of the ground is to enhance downforce. For the same reasons, the maximum and the minimum downforce values are different, but they occur at symmetrical positions with respect to the mean position, so that the lag is $0.50T$. Furthermore, this also proves that the decrease in $\hat{h}_{Cl\max}$ with frequency is not due to the stall of the airfoil. $\alpha_{\text{eff,max}}$ increases with frequency, reaching values of the order of $\alpha_{\text{eff,max}} \approx 25^\circ$ and $\alpha_{\text{eff,min}} \approx -15^\circ$ at $k = 4.37$. It can also be noted that, while $\alpha_{\text{eff,max}}$ increases almost linearly with frequency, $\alpha_{\text{eff},Cl\max}$ tends to constant. But the same situation is found for $\alpha_{\text{eff},Cl\min}$ (in other words, minimum downforce lags maximum downforce by $0.50T$) even though the absolute value of $\alpha_{\text{eff,min}}$ is lower than $\alpha_{\text{eff,max}}$ (and it is harder to stall on the top surface), so the cause of the decrease in $\hat{h}_{Cl\max}$ with frequency is not stall.

The influence of added mass effects on the flowfield is particularly noticeable at high frequencies, whereas at low frequencies the flowfield presents a configuration more typical of stationary airfoils (including a stagnation point at the leading edge, suction peak on the bottom surface and pressure recovery downstream). For instance, Fig. 12 shows how the pressure distribution around the airfoil changes dramatically with ride height at a high frequency ($k = 4.37$). Near the bottom position (upstroke), the suction peak remains near the leading edge, but with $C_p \approx -12$. Also, the suction forces are quite high along the entire bottom surface, leading to a big discontinuity between upper and lower surfaces near the trailing edge. The pressure recovery occurs along the finite trailing edge. But arguably the most interesting aspect is the trail left by the airfoil as it moves, leaving a hole of air in the space just emptied (below) and pushing the flow out of its path as it occupies its space (above). The result is an area of low pressure below the airfoil and an area of high pressure above the airfoil. Remarkably, the domain of influence of the motion of the airfoil is not limited to the boundary-layer region (as is the case in a stationary airfoil), but extends to a vertical distance of one chord length away from the body. As the airfoil moves up, the pressure on the bottom surface increases and that on the top surface decreases, starting from the trailing edge and moving upstream with decreasing acceleration. At the top position, the pressure forces are inverted on most of the chord length (from $x/c = 0.14$) and net negative downforce is produced. Between the top and the mean position, there is a pressure peak instead of a suction peak on the lower surface. Downforce is acting upward due to the negative acceleration, but the pressure profile is fundamentally different from the resulting counterpart, due to positive acceleration. Again this is a direct consequence of the profile and incidence. The downstroke consists of the pressure distribution reversing again to restore the original suction on bottom/pressure on top combination. At the bottom position there is no peak, but a relatively constant suction surface, which leads to a very uniform downforce distribution along the chord. The pressure distribution offers a notable insight into the

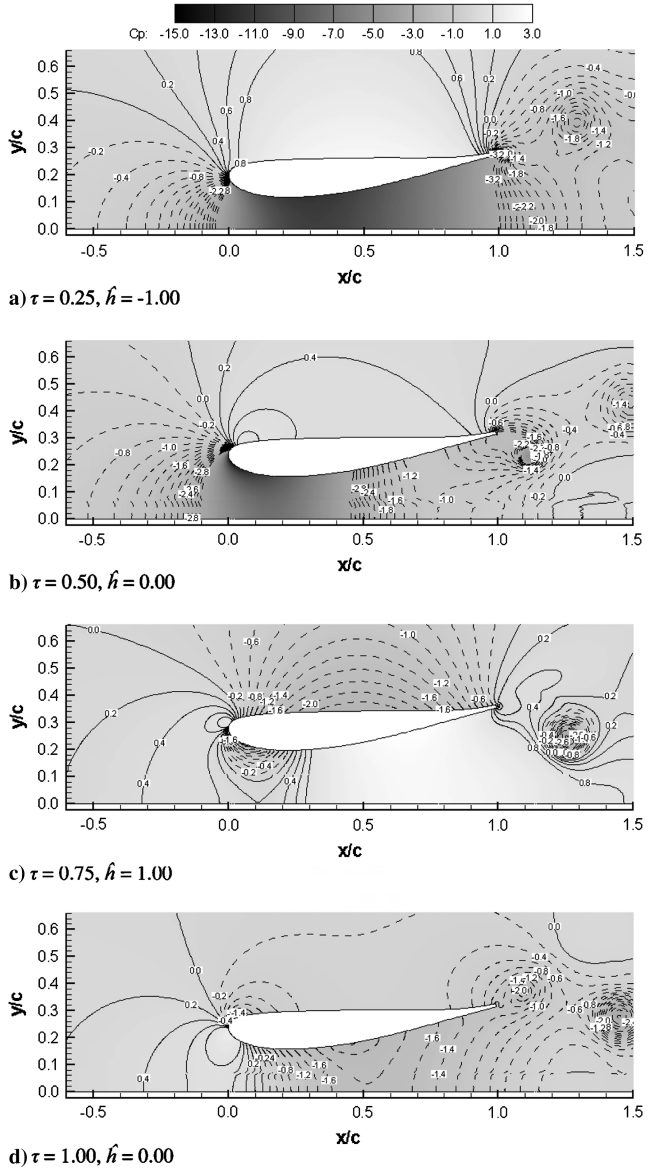

Fig. 12 Contours of pressure coefficient C_p in region 3 at $k = 4.37$.

effects of added mass, but most important, one should remember that the general pattern is independent of ground distance, albeit the effect is reinforced by ground proximity.

Finally, it is worth mentioning that forced shedding at the heaving frequency occurs in this regime in the form of a reverse Kármán vortex street. While this shedding process is inviscid and due to the abrupt change in α_{eff} at the mean position at high frequencies, natural shedding, which could be apparent at low frequencies, is a viscous phenomena that does not occur for this airfoil at this Reynolds number. Instead, the wake flaps in sync with the motion of the airfoil.

VI. Conclusions

This numerical simulation of an inverted airfoil placed close to the ground under oscillation aimed to investigate the differences between the dynamic motion and that of a stationary airfoil. In addition to the well-known mechanism of ground effect for a stationary airfoil, the unsteady motion provides two new mechanisms that govern the flow at different regimes.

The three mechanisms are as follows:

1) The *ground effect* occurs at low frequencies and the flow can be considered quasi-stationary; thus, its configuration is given by the stationary results at each ride height. In the force enhancement region, more downforce is generated when the airfoil is closer to the ground. In the force reduction region, downforce is generated away from the ground. When the airfoil covers part of both regions, there will be a maximum downforce at a ride height that corresponds to the boundary between both regions. Ground effect does not appear in freestream.

2) The *incidence effect* occurs at medium frequencies when the flow is no longer quasi-stationary, but is also apparent at low frequencies in freestream. There is an effective incidence due to the vertical velocity of the airfoil and the flow configuration is set by the equivalent pitching motion. Separation due to ground proximity is enhanced by increasing incidence as the frequency becomes larger. Close to the ground the contribution of incidence effect might not prevail over ground effect.

3) The *added mass effect* is prominent at very high frequencies, resulting in downforce being directly proportional to the vertical acceleration. This effect is inviscid and independent of ground proximity. The pressure distribution around the airfoil markedly changes through the cycle, leading to an inverted pressure distribution at some ride heights and large variations in downforce, involving negative values of downforce.

Based on the location of the maximum downforce in the cycle of oscillation, in terms of nondimensional displacement from the mean position, three regimes have been proposed. The relative contribution of each mechanism to the flow configuration varies through each regime:

1) In *regime a* the maximum downforce moves from the bottom to a maximum position that depends on the region, but that tends to be at high effective incidence. The maximum is displaced to higher frequencies as the mean ride height gets closer to the ground, due to stronger separation at low frequencies where viscous effects are important. Down to a certain mean ride height, the flow transits from a ground effect to an incidence effect dominated flow. Closer to the ground, the incidence effect is never the whole contributor, due to the strength of ground effect.

2) In *regime b* the maximum downforce moves from the maximum down to low positions where the added mass effect is important. The flow configuration becomes inviscid and the ground influence disappears.

3) In *regime c* the position of the maximum downforce barely changes with frequency. The flow is mainly inviscid and independent of ground distance.

Finally, it has been proven that the flow configuration depends mainly on the reduced frequency, except for the boundary-layer thickness that grows with reduced Reynolds number. The magnitude of the forces is weakly influenced by Reynolds number. However, the mechanisms and regimes described are solely a function of k.

Appendix A: Effect of Freestream Velocity

In addition to varying the frequency of oscillation, the reduced frequency can also change by means of a second independent parameter: the freestream velocity. A wing might be flapping at a constant frequency (due to natural vibration or a constant secondary effect) while its horizontal velocity changes. It is the case of a racing car on a straight: the car covers a wide range of velocities while the frequency of oscillation remains mostly fixed. If the results depend only on k and not on f or U_∞ alone, then the motion will be a function of one independent parameter instead of 2 (k and Reynolds number). Note that the third independent parameter a/c is not considered in this study, but it has been well documented in other papers [16,18,19].

The effect of Reynolds number on a stationary airfoil under fully turbulent conditions is mainly visible on the boundary layer. Increasing the Reynolds number results in a thinner boundary layer, delayed separation, and reduced viscous effects. This can be extended to the dynamic case, in which the Reynolds number variation can be noted in the boundary-layer thickness, as seen in the comparison of vorticity contours at $k = 4.37$ shown in Fig. A1, for the same k and different Reynolds numbers. Aside from a small region inside the boundary layer, the flow pattern and nondimensional quantities are identical in all three cases. Likewise, the

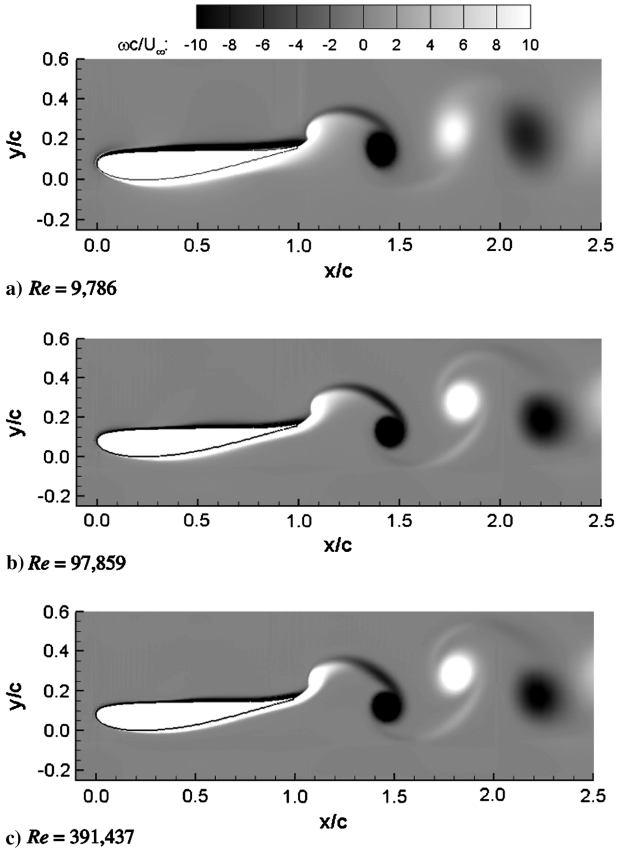

Fig. A1 Contours of nondimensional vorticity in region 0 at $k = 4.37$, $\tau = 1.00$, and $\hat{h} = 0.00$.

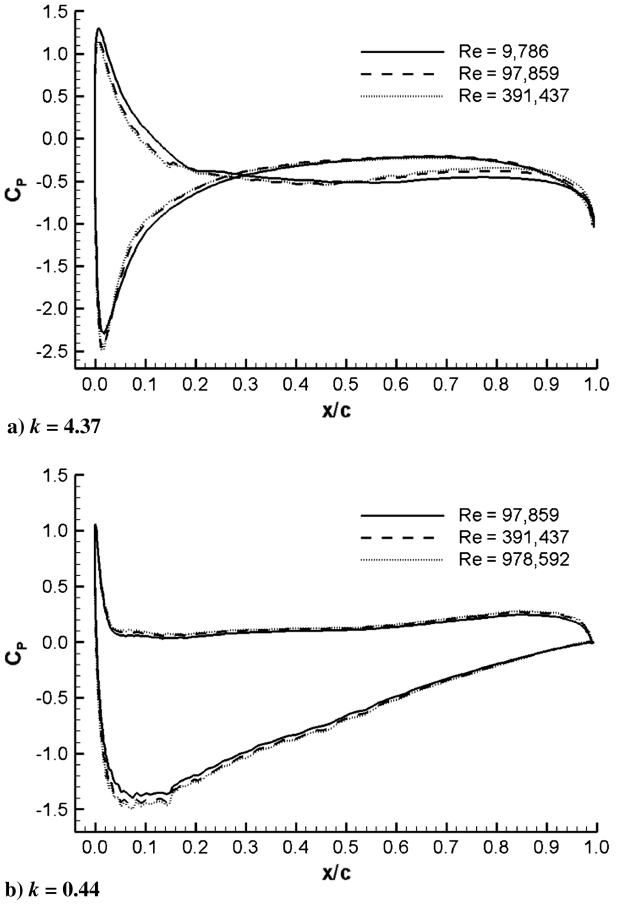

Fig. A2 Surface pressure distribution in region 0 for various Reynolds numbers at $\tau = 1.00$ and $\hat{h} = 0.00$.

pressure distribution plotted in Fig. A2a is akin for all Reynolds numbers, except for the suction peak and stagnation point at $Re = 9786$, which have a slightly higher pressure. This results in a small difference on the pressure and suction recovery and in a higher suction toward the trailing edge. Nonetheless, the forces match each other: $C_L = -0.20$, -0.17, and -0.18 for $Re = 9786$, 97,859, and 391,437, respectively.

For $k = 0.44$, Fig. A2b shows that the main difference is located in the suction region, which decreases for the lowest Reynolds number (in this case, $Re = 97,859$). Despite the difference in Reynolds number and boundary-layer thickness (Fig. A3), the change in downforce is very small: $C_L = 0.80$, 0.85, and 0.87 for $Re=$ 97, 859, 391,437, and 978,592, respectively.

Regarding the phase lag, Fig. A4 presents the curves for three different frequencies. Each curve was obtained by varying the Reynolds number at a constant f. They match each other perfectly, regardless of Reynolds number, proving that the mechanisms that affect the flow are exclusively dependent on k.

Analysis of the other regions lead to the same conclusion: the Reynolds number has a small influence on the quantitative values, but not on the physical configuration of the flow, which is dictated by the reduced frequency.

From a purely theoretical point of view, it is possible to derive this dependence for each mechanism. When the ground effect is dominant, $k \to 0$ and the flow is considered to be quasi-stationary, so the dynamic motion is not relevant. The problem simplifies to a direct application of ground effect theory.

For higher frequencies, when incidence and added mass effects are important, Theodorsen's theory [i.e., Eq. (5)] can be employed to obtain the lift coefficient:

$$C_L = \frac{L}{1/2\rho U_\infty^2 c} = \frac{2\pi\rho U_\infty^2}{1/2\rho U_\infty^2 c}\left[-\frac{k^2}{2} - Gk + iFk\right] a e^{i2\pi ft}$$
$$= 4\pi\left[-\frac{k^2 a}{2c} - G\frac{ka}{c} + iF\frac{ka}{c}\right] e^{i2\pi\tau} \tag{A1}$$

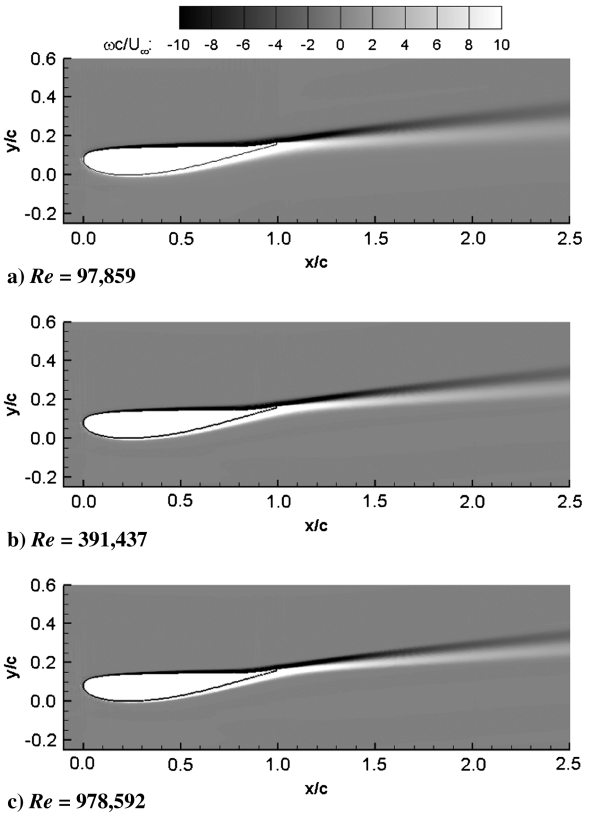

Fig. A3 Contours of nondimensional vorticity in region 0 at $k = 0.44$, $\tau = 1.00$, and $\hat{h} = 0.00$.

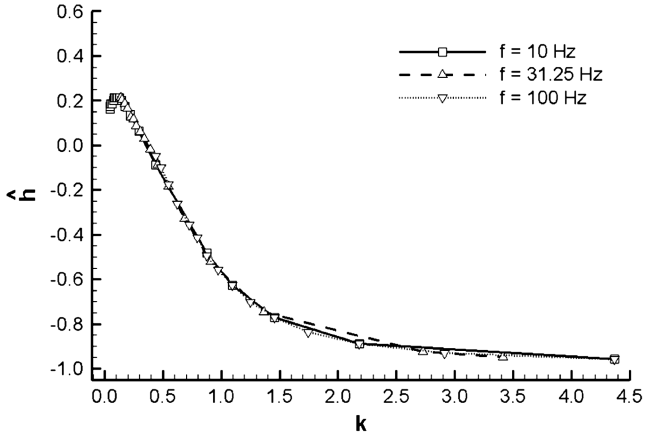

Fig. A4 Variation of position of maximum downforce with reduced frequency in region 0 for various frequencies.

which is a function of the reduced frequency k, the amplitude a/c, and the nondimensional time τ. Since a/c is constant in this study, the time-dependent lift coefficient depends on k. Although Theodorsen's theory applies to inviscid flow, the solution for viscous flow is expected to be similar based on the results shown before. The effect of Reynolds number was shown to be of secondary importance, particularly regarding the phase lag.

Acknowledgments

The authors would like to thank Brawn GP for their support: in particular, David Jeffrey, Jonathan Zerihan, and Jonathan Eccles.

References

[1] Shyy, W., "Special Issue on Animal Locomotion in Fluids, and Its Mimicry," *Applied Mechanics Reviews*, Vol. 58, No. 4, 2005, pp. 225–301.
doi:10.1115/1.1943432

[2] Abate, G., Ol, M., and Shyy, W., "Introduction: Biologically Inspired Aerodynamics," *AIAA Journal*, Vol. 46, No. 9, 2008, pp. 2113–2114.
doi:10.2514/1.35949

[3] Shyy, W., Lian, Y., Tang, J., Viieru, D., and Liu, H., *Aerodynamics of Low Reynolds Number Flyers*, Cambridge Aerospace Series, Cambridge Univ. Press, New York, 2008.

[4] Theodorsen, T., "General Theory of Aerodynamic Instability and the Mechanism of Flutter," NACA TR-496, 1935.

[5] Andro, J.-Y., and Jacquin, L., "Frequency Effects on the Aerodynamic Mechanisms of a Heaving Airfoil in a Forward Flight Configuration," *Aerospace Science and Technology*, Vol. 13, No. 1, 2009, pp. 71–80.
doi:10.1016/j.ast.2008.05.001

[6] Zerihan, J., and Zhang, X., "A Single Element Wing in Ground Effect; Comparison of Experiments and Computation," AIAA Paper 2001-0423, 2001.

[7] Dominy, R. G., "Aerodynamics of Grand Prix Cars," *Proceedings of the Institution of Mechanical Engineers. Part D, Journal of Automobile Engineering*, Vol. 206, No. D4, 1992, pp. 267–274.
doi:10.1243/PIME_PROC_1992_206_187_02

[8] Zerihan, J., and Zhang, X., "Aerodynamics of a Single Element Wing in Ground Effect," *Journal of Aircraft*, Vol. 37, No. 6, 2000, pp. 1058–1064.
doi:10.2514/2.2711

[9] Zhang, X., and Zerihan, J., "Turbulent Wake Behind a Single Element Wing in Ground Effect," *Proceedings of the 10th International Symposium on Applications of Laser Techniques to Fluid Mechanics*, Lisbon, Portugal, July 2000.

[10] Zhang, X., and Zerihan, J., "Off-Surface Aerodynamic Measurement of a Wing in Ground Effect," *Journal of Aircraft*, Vol. 40, No. 4, 2003, pp. 716–725.
doi:10.2514/2.3150

[11] Garrick, I. E., "Propulsion of a Flapping and Oscillating Airfoil," NACA TR-567, 1936.

[12] Von Kármán, T., and Burgess, J. M., *Aerodynamic Theory*, Springer, Berlin, 1934.

[13] Knoller, R., "Die Gesetze des Luftwiderstandes," *Flug- und Motortechnik*, Vol. 3, 1909, pp. 1–7.

[14] Betz, A., "Ein Beitrag zur Erklarung des Segelfluges," *Zeitschrift für Flugtechnik und Motorluftschiffahrt*, Vol. 3, 1912, pp. 269–272.

[15] Freymuth, P., "Propulsive Vortical Signature of Plunging and Pitching Airfoils," *AIAA Journal*, Vol. 26, No. 7, 1988, pp. 881–883.
doi:10.2514/3.9982

[16] Koochesfahani, M. M., "Vortical Patterns in the Wake of an Oscillating Airfoil," *AIAA Journal*, Vol. 27, No. 9, 1989, pp. 1200–1205.
doi:10.2514/3.10246

[17] Jones, K. D., Dohring, C. M., and Platzer, M. F., "Experimental and Computational Investigation of the Knoller–Betz Effect," *AIAA Journal*, Vol. 36, No. 7, 1998, pp. 1240–1246.
doi:10.2514/2.505

[18] Young, J., and Lai, J. C. S., "Oscillation Frequency and Amplitude Effects on the Wake of a Plunging Airfoil," *AIAA Journal*, Vol. 42, No. 10, 2004, pp. 2042–2052.
doi:10.2514/1.5070

[19] Lai, J. C. S., and Platzer, M. F., "Jet Characteristics of a Plunging Airfoil," *AIAA Journal*, Vol. 37, No. 12, 1999, pp. 1529–1537.
doi:10.2514/2.641

[20] Young, J., and Lai, J. C. S., "Vortex Lock-In Phenomenon in the Wake of a Plunging Airfoil," *AIAA Journal*, Vol. 45, No. 2, 2007, pp. 485–490.
doi:10.2514/1.23594

[21] Moryossef, Y., and Levy, Y., "Effect of Oscillations on Airfoils in Close Proximity to the Ground," *AIAA Journal*, Vol. 42, No. 9, 2004, pp. 1755–1764.
doi:10.2514/1.6380

[22] Minotti, F. O., "Unsteady Two-Dimensional Theory of a Flapping Wing," *Physical Review E (Statistical Physics, Plasmas, Fluids, and Related Interdisciplinary Topics)*, Vol. 66, No. 5, 2002, Paper 051907.
doi:10.1103/PhysRevE.66.051907

[23] Mahon, S. A., "The Aerodynamics of Multi-Element Wings in Ground Effect," Ph.D. Thesis, School of Engineering Sciences, Univ. of Southampton, Southampton, England, U.K., 2005.

[24] Spalart, P. R., and Allmaras, S. R., "A One-Equation Turbulence Model for Aerodynamic Flows," AIAA Paper 92-0439, 1992.

[25] Zerihan, J., "An Investigation into the Aerodynamics of Wings in Ground Effect," Ph.D. Thesis, School of Engineering Sciences, Univ. of Southampton, Southampton, England, U.K., 2001.

[26] Nishino, T., Roberts, G. T., and Zhang, X., "Unsteady Rans and Detached-Eddy Simulations of Flow Around a Circular Cylinder in Ground Effect," *Journal of Fluids and Structures*, Vol. 24, No. 1, 2008, pp. 18–33.
doi:10.1016/j.jfluidstructs.2007.06.002

[27] Sunada, S., Kawachi, K., Matsumoto, A., and Sakaguchi, A., "Unsteady Forces on a Two-Dimensional Wing in Plunging and Pitching Motions," *AIAA Journal*, Vol. 39, No. 7, 2001, pp. 1230–1239.
doi:10.2514/2.1458

[28] Fung, Y. C., "Fundamentals of Flutter Analysis," *An Introduction to the Theory of Aeroelasticity*, Wiley, New York, 1955.

M. Visbal
Associate Editor